RSC Advances

PAPER

View Article Online
View Journal | View Issue

Cite this: *RSC Adv.*, 2021, **11**, 14527

Exploration of the cofactor specificity of wild-type phosphite dehydrogenase and its mutant using molecular dynamics simulations†

Kunlu Liu,‡[a] Min Wang,‡[a] Yubo Zhou,[b] Hongxiang Wang,[b] Yudong Liu,[b] Lu Han*[a] and Weiwei Han *[a]

Received 11th January 2021
Accepted 13th April 2021

DOI: 10.1039/d1ra00221j

rsc.li/rsc-advances

Phosphite dehydrogenase (Pdh) catalyzes the NAD-dependent oxidation of phosphite to phosphate with the formation of NADH. It can be used in several bioorthogonal systems for metabolic control and related applications, for example, bioelectricity. At present, NAD has poor stability at high concentrations and costs are expensive. Implementation of a non-natural cofactor alternative to the ubiquitous redox cofactor nicotinamide adenosine dinucleotide (NAD) is of great scientific and biotechnological interest. Several Pdhs have been engineered to favor a smaller-sized NAD analogue with a cheaper price and better thermal stability, namely, nicotinamide cytosine dinucleotide (NCD). However, the conformational changes of two cofactors binding to Pdh remain unknown. In this study, five molecular dynamics (MD) simulations were performed to exploit the different cofactors binding to wild-type (WT) Pdh and mutant-type (MT) Pdh (I151R/P176E/M207A). The results were as follows: First, compared with WT Pdh, the cofactor-binding pocket of mutant Pdh became smaller, which may favor a smaller-sized NCD. Second, secondary structure analysis showed that the alpha helices in residues 151–207 partly disappeared in mutant Pdh binding to NAD or NCD. Our theoretical results may provide a basis for further studies on the Pdh family.

1. Introduction

Phosphite dehydrogenase (Pdh) catalyzes the NAD-dependent oxidation of phosphite to phosphate with the formation of NADH.[1–11] This kind of enzyme regeneration module is combined with a coenzyme-consuming reaction module to achieve the ideal coenzyme balance in multi-enzyme molecular machines. The multi-enzyme reaction sometimes takes place at high temperature, NAD and NAD(P)H may be decomposed, which results in the decrease of coenzyme concentration during the operation of the multi-enzyme molecular machine *in vitro*, thereby affecting the catalytic efficiency of Pdh. Moreover, NAD is expensive and less specific. Implementation of a non-natural cofactor alternative to the ubiquitous redox cofactor nicotinamide adenosine dinucleotide (NAD) is of great scientific and biotechnological interest. Thus, redox enzymes with a more stringent preference to NAD analogues (*e.g.*, NCD) needed to be developed for cheaper price and better thermal stability. They can be used in several biorthogonal systems for metabolic control and related applications, for example, bioelectricity.[12–17]

According to sequence comparisons of Pdh in the NAD^+-dependent D-2-hydroxyacid dehydrogenase family,[18,19] Pdh shares 56% identity with other members of this family. Three conserved catalytic residues have been reported to be useful for catalysis by Pdh.[19,20] A conserved histidine residue (His293 in Pdh) is proposed to act as a general base for the nucleophilic water molecule attacking on phosphite, Glu264 orients and modulates the pKa of the active site His293, and Arg237 is near the substrate, phosphite, prior to nucleophilic attack.[19,21] The site-specific mutants of residues demonstrated that the mutations were at His293, Arg237, and Glu264 severely compromises catalysis relative to the WT.[19,22]

In 2019, Zhao *et al.* made a semi-rational approach to characterize several mutant Pdh responsible for NCD-binding capability by X-ray crystallography.[1] They obtained mutants with substantially improved NCD preference.[1] Although more and more synthetic systems using non-natural cofactors can be treated as new tools for widespread applications by chemical and synthetic biologists, some issues remain to be elucidated. For example, the conformational changes of two cofactors binding to Pdh remain unknown.

In this study, five MD simulations were performed to explore the different cofactors binding to WT Pdh and MT Pdh. This study will provide useful information to address challenging problems for chemical and synthetic biologists.

[a]*Key Laboratory for Molecular Enzymology and Engineering of Ministry of Education, School of Life Science, Jilin University, 2699 Qianjin Street, Changchun 130012, China. E-mail: luhan@jlu.edu.cn; weiweihan@jlu.edu.cn*

[b]*High School Attached to Northeast Normal University, 506 Ziyou Road, Changchun 130012, China*

† Electronic supplementary information (ESI) available. See DOI: 10.1039/d1ra00221j

‡ These authors contributed equally to this work.

2. Materials and methods

2.1. Preparation of the protein structures

Five different systems were used to identify the binding mechanism with Pdh: (1) free Pdh, (2) WT Pdh_NCD, (3) MT Pdh_NCD, (4) WTPdh_NAD, and (5) MT Pdh_NAD. The initial coordination of Pdh with NCD was obtained from the Protein Data Bank (PDB) (PDB code 6IH3).[1] The 3D structure of NAD was obtained from PDB (PDB code 4E5N). The MT Pdh were generated using Pymol. Protonation states were conducted at physiological pH by using the H^{++} server (http://biophysics.cs.vt.edu/index.php). All residues were assigned in their standard protonation (pH = 7), and all missing hydrogen atoms were generated using Discovery Studio 4.0 client software. NCD and NAD were then optimized according to the density functional theory at the B3LYP/6-31G* level[23] by using Gaussian 09 software.[24]

2.2. Molecular docking

NAD was docked to Pdh with AutoDock Vina software.[25,26] AutoDockTools were used for docking. We adjusted the box to the centre of the primary and secondary binding sites. The three-dimensional grids were set as 46 × 40 × 36 points with a grid spacing of 1 Å. NAD was docked to Pdh in the binding pocket, and the corresponding energy evaluations were also generated. The most popular and stable docking conformations were selected as the initial binding modes for the subsequent MD simulations.

2.3. MD simulation

Gromos 53A6 force field[27,28] was applied to describe proteins (WT and MT) and ligands (NAD and NCD). The parameterization of the two ligands was produced by the PRODRG2.5 server. All of the systems were subjected to MD simulations by using a SPC water model in a periodic box.[29] Chloride and sodium ions were added to a random location as a replacement for the water molecules in the simulation box to neutralize the systems. Energy minimization was performed using the steepest descent method to equilibrate the initial structure. Afterward, 100 ps NVT (constant number of particles, volume, and temperature) and 100 ps NPT were adopted to stabilize the environment of the systems at 300 K and 1 bar. The coupling constant was set to 0.1 and 2.0 ps for temperature and pressure. The MD simulations were performed using the GROMACS 4.5.2 software package[30,31] on the basis of the predicted complexes generated by AutoDock Vina.[25,26] During the 200 ns simulation, the LINCS algorithm[32] was employed to fix all of the bonds, and the long-range electrostatics was computed by the particle mesh Ewald method[33] with a grid spacing of 0.16 nm.

2.4. Cross-correlation analysis and principal component analysis (PCA)

Bio3D version 2.3.0 was used to perform cross-correlation analysis. The coordinate axis scales indicated the atomic number in the covariance matrix map. PCA can provide a detailed picture of biomolecular motion to identify large-scale motions and the correlated movements of biological protein systems. In this study, PCA was visualized by VMD version 1.9.3. The energy of macromolecular conformations such as the first two principal components (PC1, PC2) were characterized in free energy landscape (FEL). FEL is used to describe the energies of sets of macromolecular conformations.[34,35]

3. Results and discussion

3.1. Quantum chemical calculations and structural stability of the five systems

Pdh has drawn attention because it can be used as a cofactor regeneration system for the transfer of NAD^+ to NADH in cofactor recycling. Moreover, due to their relatively inexpensive substrate (*i.e.*, phosphite) and high catalytic efficiency, Pdhs are attractive candidates in the enzymatic regeneration of NADH from NAD^+.[36–41]

X-ray crystallographic analysis revealed that Pdh has two catalytic domains in Fig. 1. His293, Asp261, Val262, Ala235, Gly295, Val262, Ala235, Gly295, Thr104, Ser296, Leu100, Lys76, Val156, Thr101, Gly157, Ala155, Gly154, Met153, Ile177, Asp175, Gly152, Pro176, Thr214, Val208, Pro209, Lys188, Met207, and Cys236 (important residues for NCD binding) were shown in Fig. S1.† NAD was docked to WT Pdh and MT Pdh (Fig. 1d and 2).

The most popular and stable docking conformations were selected. It was well known that molecular docking was determined not only by the highest score conformation but also by the orientation. See Fig. S2,† it can be seen that the lowest energy docked complexes (NAD) were similar to the reference (NCD). Fig. 2a showed that Gly295, His293, Ala235, Met207, Cys236, Pro209, Val208, Pro209, Val262, Arg237, Val156, Ala155, Gly154, Cys174, Ile177, Cys174, Asp175, and Pro176 were important residues for NAD binding to WT Pdh. In MT Pdh_NAD, Arg151,

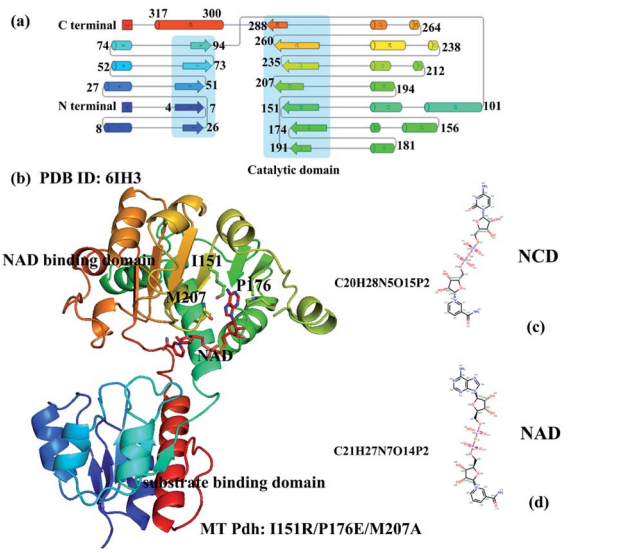

Fig. 1 Structure of the complex. (a) 2D structure topology, (b) 3D structure of Pdh (PDB code 6IH3), (c) structure of NCD, (d) structure of NAD.

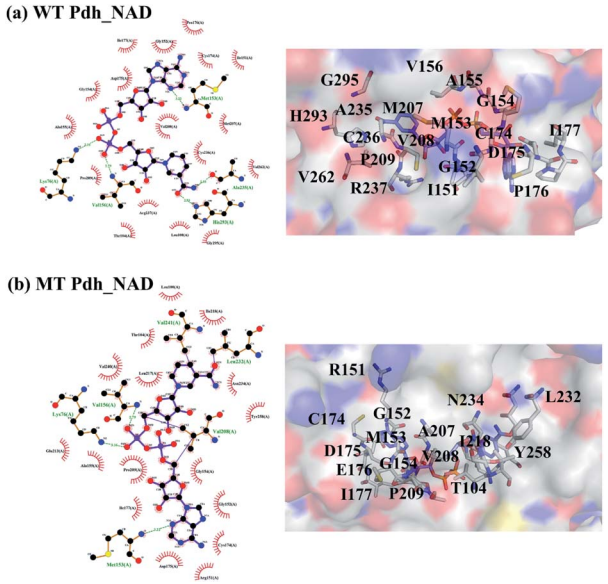

Fig. 2 The docked pose of Pdh_NAD. (a) The docked pose of WT Pdh_NAD, (b) the docked pose of MT Pdh_NAD.

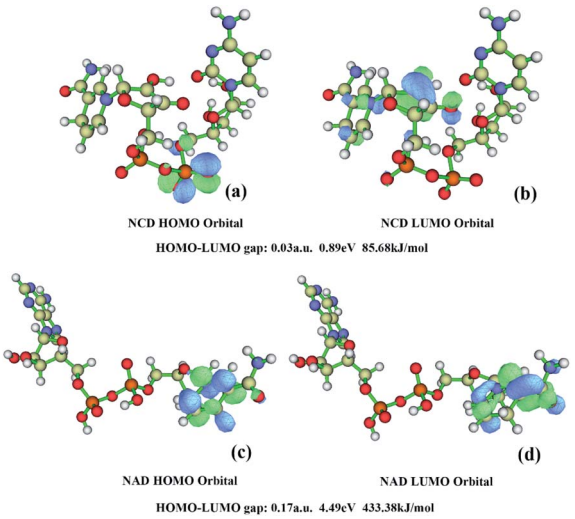

Fig. 3 Quantum chemical calculations. (a) HOMO orbital of NCD, (b) LUMO orbital of NCD, (c) HOMO orbital of NAD, (d) LUMO orbital of NAD.

Cys174, Asp175, Glu176, Ile177, Gly152, Met153, Gly154, Pro209, Ala207, Asn208, Asn234, Ile218, Thr104, Tyr258, and Leu232 were in the NAD binding pocket. The active residues for NAD and NCD binding to Pdh were different. The reason may be lay in the different size of NAD and NCD.

Quantum chemical calculation was used on two ligands by using Gaussian 09(ref. 24) to optimize the structures. The differences in energy between these HOMO and LUMO frontier orbitals can be used to predict the strength and stability of electron transfer.[42] Fig. 3 showed the HOMO and LUMO orbits drawn by the Multiwfn program.[43] E_{gap} is the energy differences between HOMO and LUMO orbits. In terms of E_{gap}, the

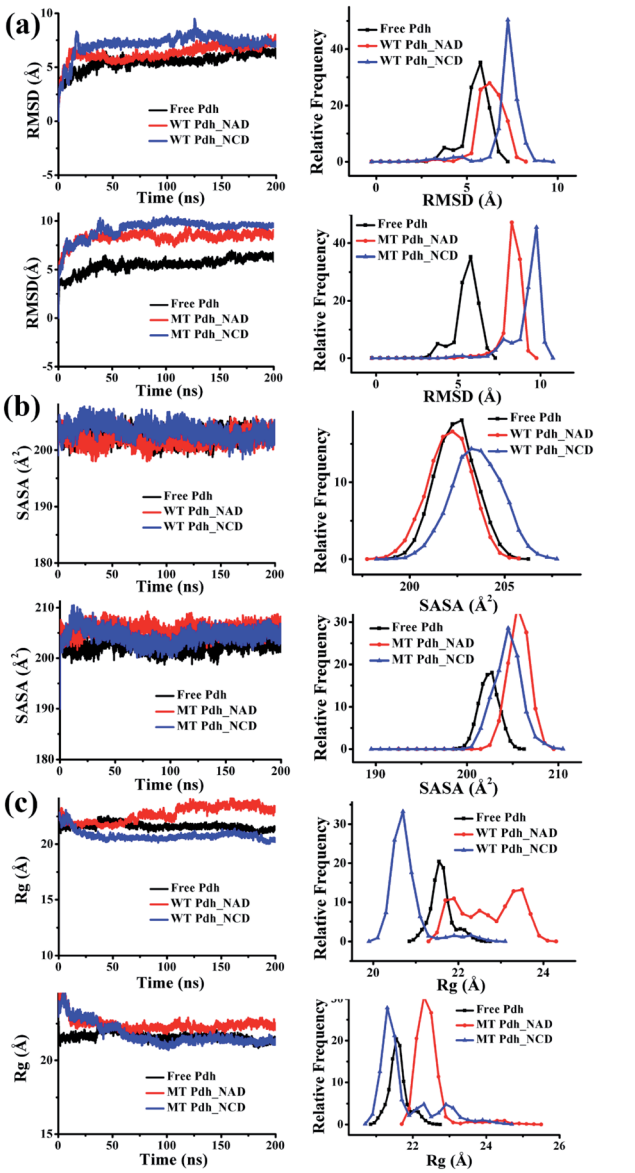

Fig. 4 Structural stability of the five systems during 200 ns simulations. (a) RMSD plot, (b) SASA plot, (c) R_g plot.

cofactors NCD had smaller energy than that of NAD, indicating that electron transfer might occur more easily in NCD than in NAD. Therefore, NCD had more interactions than NAD, including H bonds, salt bridges, and Van der Waals' force (VDW) interactions.

After 200 ns simulations, the root-mean-square deviations (RMSDs) of the C_α atom backbone of the five systems were calculated during simulations in Fig. 4. As shown in Fig. 4a, the RMSDs of free Pdh and WT Pdh_NAD could be stabilized at 6 Å, and that of WT Pdh_NCD could be stabilized at 7.5 Å, indicating that the structures of the three systems already reached a state of relative equilibrium. Meanwhile, the RMSDs of MT Pdh_NAD and MT Pdh_NCD could be stabilized at approximately 9 Å after 20 ns, suggesting that the structures of the two systems reached a state of relative equilibrium.

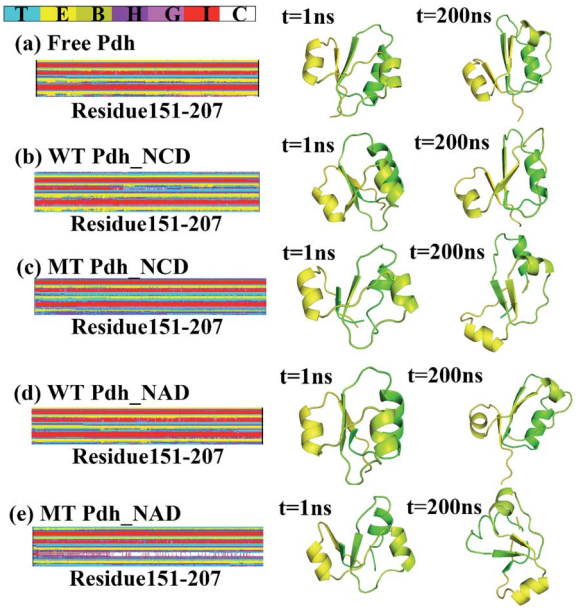

Fig. 5 Secondary structure analysis. (a) Free Pdh, (b) WT Pdh_NCD, (c) MT Pdh_NCD, (d) WT Pdh_NAD, (e) MT Pdh_NAD. T: turn, E: extended conformation, B: isolated bridge, H: alpha helix, G: 3-10 helix, I: pi-helix, C: coil.

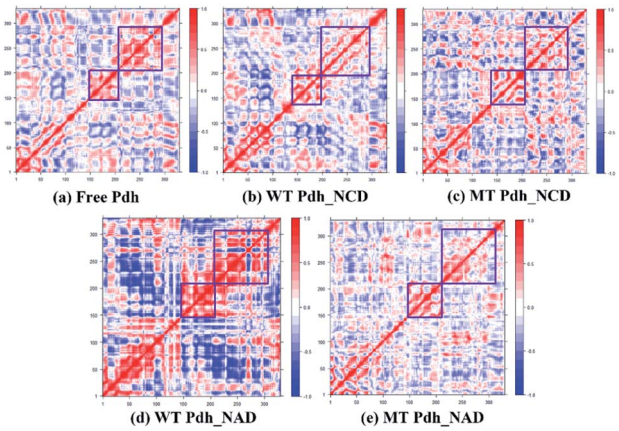

Fig. 6 Residue cross correlation analysis. (a) Free Pdh, (b) WT Pdh_NCD, (c) MT Pdh_NCD, (d) WT Pdh_NAD, (e) MT Pdh_NAD.

Table 2 The probability (%) of PC1 and PC2 during MD simulations

	PC1	PC2
Free Pdh	32.26	18.72
WT Pdh_NCD	34.12	18.35
MT Pdh_NCD	52.35	14.46
WT Pdh_NAD	63.16	9.12
MT Pdh_NAD	27.81	19.34

The solvent-accessible surface area (SASA) of the five systems was calculated by the VMD program. The SASA of residues to find the points on a sphere that were exposed to solvent. In Fig. 4b, the WT Pdh_NCD complex became larger than WT Pdh_NAD. In MT Pdh, MT Pdh_NAD became larger than MT Pdh_NCD, suggesting that the SASA of MT Pdh_NCD was smaller.

The radius gyration (R_g) of the five systems was calculated by the VMD program. In Fig. 4c, the R_g values of WT Pdh_NAD could be stabilized at 20 Å, and those of WT Pdh_NCD could be stabilized at 22 Å after 20 ns. As shown in Fig. 4c, the R_g values of MT Pdh_NAD and free Pdh can be stabilized at 22 Å, and those of MT Pdh_NCD can be stabilized at 21 Å after 20 ns. This finding may facilitate the conformational rearrangement of the NAD binding domain in the MT Pdh to move to the catalytic domain in the MT Pdh_NCD complex.

3.2. Conformational changes caused by two cofactor binding to WT and MT Pdh

The conformational changes caused by the five systems were investigated and compared. To investigate the conformational changes, we obtained the differences in the secondary structure (DSSP) by using the do_dssp command. The DSSP of residues 151–207 in MT Pdh differed from that in free Pdh and WT Pdh significantly (Fig. 5). As shown in Fig. 5c and e, the alpha helices in residues 151–207 partly disappeared in MT Pdh binding to NAD or NCD. The alpha helix probability (%) of residues 154–163 of the five systems during MD simulations were shown in Table 1. Residues 154–163 all contained a helix in free Pdh and WT Pdh binding to NAD or NCD. However, the helix of MT Pdh partly disappeared. The reason may be due to the partly disappeared alpha helix, wherein the smaller cofactor, NCD, binds to MT Pdh.

3.3. Residue cross-correlation and FEL calculations

Correlation matrix analysis can promote the understanding of protein regions that have intense relevant conformational changes, which can shed light on the dynamic motion of Pdh induced by cofactor binding. In this study, covariance matrix maps were constructed on the basis of the first two eigenvectors

Table 1 The probability (%) for alpha helix (residue154–163) of the five systems during MD simulations

	G154	A155	V156	G157	R158	A159	I160	A161	Q162	R163
Free Pdh	1.85	96.19	99.04	99.99	99.99	100	99.98	99.81	95.64	90.01
WT Pdh_NCD	0.12	15.77	18.81	82.88	99.73	99.97	99.98	99.93	98.47	83.31
MT Pdh_NCD	0	0	0.65	98.84	99.39	99.76	99.88	98.67	93.26	66.51
WTPdh_NAD	0.67	88.50	99.49	99.99	100	100	99.81	99.89	97.41	83.15
MT Pdh_NAD	0	0	0	0.42	2.75	4.57	10.29	10.19	8.62	6.88

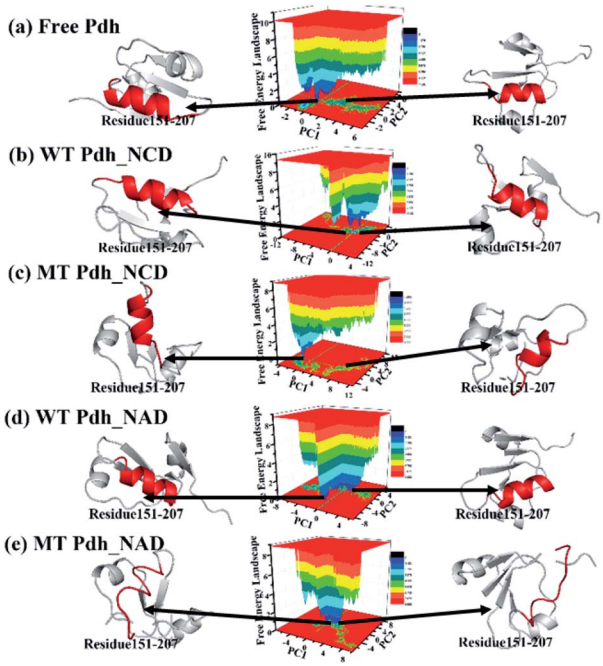

Fig. 7 Principal component analysis. (a) Free Pdh, (b) WT Pdh_NCD, (c) MT Pdh_NCD, (d) WT Pdh_NAD, (e) MT Pdh_NAD.

to depict the linear correlations of each pair of C_α atoms during the MD simulations. The matrix maps of the five systems indicated that significant motions, correlated or noncorrelated, mainly occurred among the regions of residues 150–200 and residues 200–300. Particularly, the motion in residues 151–207 deserved more attention (Fig. 6), because it occurred near the cofactor active site.

The probabilities of PC1 and PC2 of the five systems were shown in Table 2. The two most stable conformations of the Pdh structure in the five systems were shown in the left and right panels in Fig. 7. Residues 154–163 all contained a helix in free Pdh, WT Pdh_NAD, and WT Pdh_NCD. However, in MT Pdh_NAD and MT Pdh_NCD, the alpha helix partly disappeared.

PCA was used to confirm whether conformational changes were stable or not. The FEL calculations were shown in Fig. 7. In the FEL of the five systems, the different energies of the corresponding structures were shown in different colours. The conformations found in the blue area were more stable and had lower energy states than those found in the red area.

3.4. Structural stability of the cofactor-binding pocket

The RMSD, SASA, R_g, and relative frequency of residues 151–207 were also calculated in Fig. 8. The changes of the data indicated that the structure in residues 151–207 in WT Pdh with NAD or NCD was different compared with that in MT Pdh with the cofactors.

POCASA[44] (http://altair.sci.hokudai.ac.jp/g6/service/pocasa/) was used to calculate the binding pocket size during MD simulations (Parameters were listed as follow: The radius of probe sphere value was 2 Å. Single Point Flag value was 16,

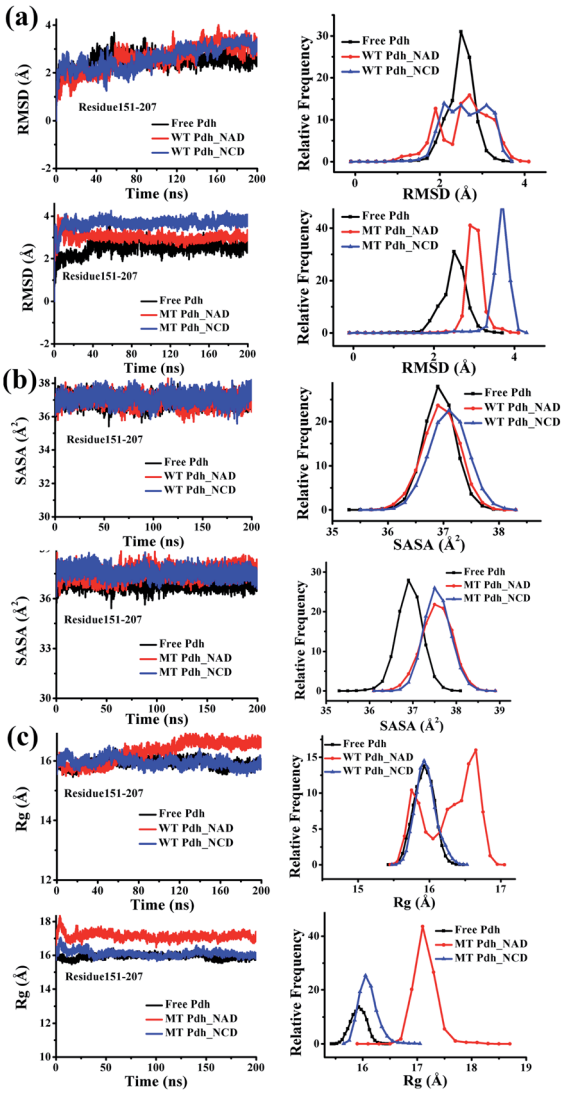

Fig. 8 Structural stability of the cofactor-binding pocket during 200 ns simulations. (a) RMSD plot, (b) SASA plot, (c) R_g plot.

Protein Depth Flag value was 18. The number of results to show was 5. The size of unit grid was 1 Å. The type of atom was all).

The binding pocket conformations of the four systems at 0, 50, and 200 ns were shown in Fig. 9. The volume of the pockets in WT Pdh_NAD was smaller than that in WT Pdh_NCD (Fig. 9a and b), the volume of the pockets in MT Pdh_NAD was larger than that in MT Pdh_NCD (Fig. 9c and d). A small cofactor-binding pocket will be useful for NCD, a small-sized cofactor, to bind to MT Pdh.

The distances between Glu264N and Asn234OD1 of the three systems including free Pdh, MT Pdh_NAD, and MT Pdh_NCD were calculated in Fig. 10. As shown in Fig. 10a, only the distance between Glu264N and Asn234OD1 in the MT Pdh_NCD complex was stabilized within 4 Å after 50 ns. Thus, the introduction of new hydrophobic interactions or hydrogen bonds in MT Pdh_NCD can be used to improve its catalytic efficiency.

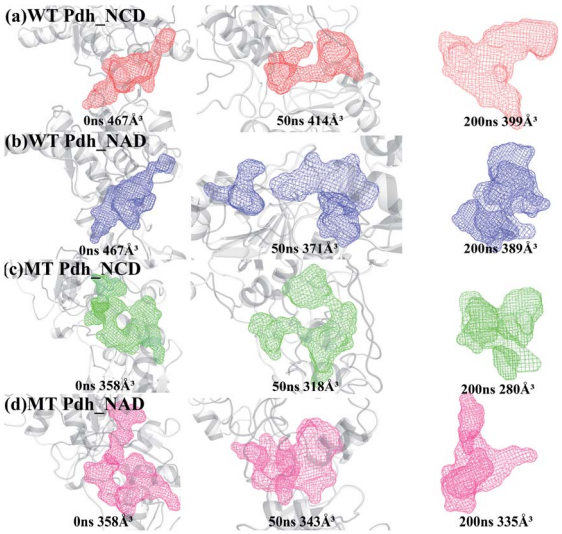

Fig. 9 The active pocket size of the four systems at 0 ns,50 ns and 200 ns MD simulations. (a) WT Pdh_NCD, (b) WT Pdh_NAD, (c) MT Pdh_NCD, (d) MT Pdh_NAD.

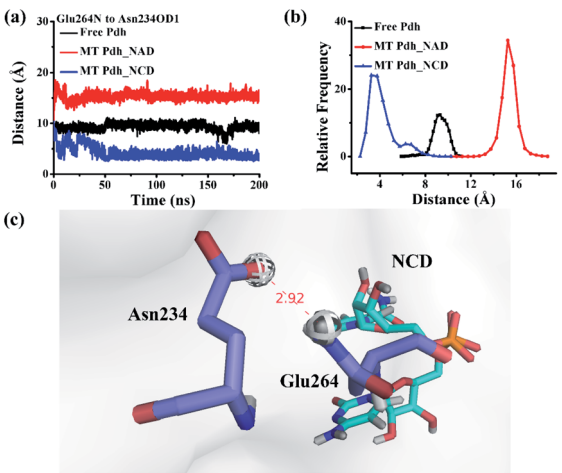

Fig. 10 The distance between Glu264N and Asn234OD1. (a) The distance between Glu264N and Asn234OD1 of Free Pdh, MT Pdh_NAD and MT Pdh_NCD, (b) relative frequency of Free Pdh, MT Pdh_NAD and MT Pdh_NCD, (c) 3D structure of the distance.

4. Conclusions

Several Pdhs have been engineered to favor a smaller-sized NAD analogue (*i.e.*, NCD). However, the conformational changes of two cofactors binding to Pdh remain unknown. In this study, five MD simulations were performed to exploit the different cofactors binding to WT Pdh and MT Pdh. The results were as follows: First, compared with WT Pdh, the cofactor-binding pocket of MT Pdh became smaller, which may favour a smaller-sized NCD. Second, secondary structure analysis showed that the alpha helices in residues 151–207 partly disappeared in MT Pdh binding to NAD or NCD. The MT Pdh moved inward the cofactor-binding pocket, which presents a more restricted region and a compact cavity, indicating an increased NCD preference. These structural data reveal that the cofactor-binding pocket of Pdh became more crowded upon the introduction of large and polar residues such as Arg or Glu. Moreover, these mutations also led to the reorientation of skeletal amino acid residues inward to narrow the binding cleft. However, these charged side chains provided additional interactions with NCD. Together, these structural changes created a compacted cofactor-binding pocket and molecular interactions beneficial to NCD residence. Our theoretical results may provide a basis for further studies on Pdh.

Conflicts of interest

There are no conflicts to declare.

Acknowledgements

This work was supported by the National Natural Science Foundation of China [31870201] and the Overseas Cooperation Project of Jilin Province [20200101068JC]. This work was performed at the High Performance Computing Center of Jilin University.

Notes and references

1 Y. Liu, Y. Feng, L. Wang, X. Guo, W. Liu, Q. Li, X. Wang, S. Xue and Z. K. Zhao, *ACS Catal.*, 2019, **9**, 1883–1887.
2 V. Schreiber, F. Dantzer, J. C. Ame and G. De Murcia, *Nat. Rev. Mol. Cell Biol.*, 2006, **7**, 517–528.
3 M. Pittelli, L. Formentini, G. Faraco, A. Lapucci, E. Rapizzi, F. Cialdai, G. Romano and G. Moneti, *J. Biol. Chem.*, 2010, **285**, 34106–34114.
4 M. S. Bonkowski and D. A. Sinclair, *Nat. Rev. Mol. Cell Biol.*, 2016, **17**, 679–690.
5 W. Ying, *Antioxid. Redox Signaling*, 2008, **10**, 179–206.
6 K. W. Ryu, T. Nandu, J. Kim, S. Challa, R. J. Deberardinis and W. L. Kraus, *Science*, 2018, **360**, 618.
7 M. Wang, B. Chen, Y. Fang and T. Tan, *Biotechnol. Adv.*, 2017, **35**, 1032–1039.
8 D. V. Titov, V. Cracan, R. P. Goodman, J. Peng, Z. Grabarek and V. K. Mootha, *Science*, 2016, **352**, 231–235.
9 C. Del Nagro, Y. Xiao, L. Rangell, M. Reichelt and T. O'Brien, *J. Biol. Chem.*, 2014, **289**, 35182–35192.
10 A. K. Holm, L. M. Blank, M. Oldiges, A. Schmid, C. Solem, P. R. Jensen and G. M. Vemuri, *J. Biol. Chem.*, 2010, **285**, 17498–17506.
11 M. J. A. van Hoek and R. M. H. Merks, *BMC Syst. Biol.*, 2012, **6**, 22.
12 A. R. Rovira, A. Fin and Y. Tor, *J. Am. Chem. Soc.*, 2017, **139**, 15556–15559.
13 F. Hallé, A. Fin, A. R. Rovira and Y. Tor, *Angew. Chem., Int. Ed.*, 2018, **57**, 1087–1090.
14 T. Knaus, C. E. Paul, C. W. Levy, S. de Vries, F. G. Mutti, F. Hollmann and N. S. Scrutton, *J. Am. Chem. Soc.*, 2016, **138**, 1033–1039.

15 D. Ji, L. Wang, S. Hou, W. Liu, J. Wang, Q. Wang and Z. K. Zhao, *J. Am. Chem. Soc.*, 2011, **133**, 20857–20862.
16 L. Wang, D. Ji, Y. Liu, Q. Wang, X. Wang, Y. J. Zhou, Y. Zhang, W. Liu and Z. K. Zhao, *ACS Catal.*, 2017, **7**, 1977–1983.
17 D. Ji, L. Wang, Y. Zhou, W. Yang, Q. Wang and Z. K. Zhao, *Cuihua Xuebao*, 2012, **33**, 530–535.
18 G. A. Grant, *Biochem. Biophys. Res. Commun.*, 1989, **165**, 1371–1374.
19 Y. Zou, H. Zhang, J. S. Brunzelle, T. W. Johannes, R. Woodyer, J. E. Hung, N. Nair, W. A. van der Donk, H. Zhao and S. K. Nair, *Biochemistry*, 2012, **51**, 4263–4270.
20 A. M. G. Costas, A. K. White and W. W. Metcalf, *J. Biol. Chem.*, 2001, **276**, 17429–17436.
21 H. A. Relyea and W. A. van der Donk, *Bioorg. Chem.*, 2005, **33**, 171–189.
22 R. Woodyer, J. L. Wheatley, H. A. Relyea, S. Rimkus and W. A. van der Donk, *Biochemistry*, 2005, **44**, 4765–4774.
23 I. L. Rogers and K. J. Naidoo, *J. Comput. Chem.*, 2017, **38**, 1789–1798.
24 J. Z. Vilseck, J. Kostal, J. Tirado-Rives and W. L. Jorgensen, *J. Comput. Chem.*, 2015, **36**, 2064–2074.
25 N. T. Nguyen, T. H. Nguyen, T. N. H. Pham, N. T. Huy, M. V. Bay, M. Q. Pham, P. C. Nam, V. V. Vu and S. T. Ngo, *J. Chem. Inf. Model.*, 2020, **60**, 204–211.
26 T. Gaillard, *J. Chem. Inf. Model.*, 2018, **58**, 1697–1706.
27 C. Oostenbrink, A. Villa, A. E. Mark and W. F. van Gunsteren, *J. Comput. Chem.*, 2004, **25**, 1656–1676.
28 O. Guvench and A. D. MacKerell, *Methods Mol. Biol.*, 2008, **443**, 63–88.
29 N. W. Ockwig, R. T. Cygan, L. J. Criscenti and T. M. Nenoff, *Phys. Chem. Chem. Phys.*, 2008, **10**, 800–807.
30 S. Pronk, S. Páll, R. Schulz, P. Larsson, P. Bjelkmar, R. Apostolov, M. R. Shirts, J. C. Smith, P. M. Kasson, D. van der Spoel and B. Hess, *Bioinformatics*, 2013, **29**, 845–854.
31 M. J. Abraham and J. E. Gready, *J. Comput. Chem.*, 2011, **32**, 2031–2040.
32 R. Kumar, R. Maurya and S. Saran, *J. Biomol. Struct. Dyn.*, 2019, **37**, 781–795.
33 R. E. Isele-Holder, W. Mitchell and A. E. Ismail, *J. Chem. Phys.*, 2012, **137**, 174107.
34 P. O'Driscoll, E. Merenyi, C. Karmonik, R. Grossman, *Annual International Conference of the IEEE Engineering in Medicine and Biology Society*, 2014, pp. 734–737.
35 J. X. Zhu, Y. Li, J. Z. Wang, Z. F. Yu, Y. Liu, Y. Tong and W. W. Han, *Front. Chem.*, 2018, **6**, 437.
36 J. M. Vrtis, A. K. White, W. W. Metcalf and W. A. van der Donk, *Angew. Chem., Int. Ed.*, 2002, **41**, 3257–3259.
37 H. K. Chenault and G. M. Whitesides, *Appl. Biochem. Biotechnol.*, 1987, **14**, 147–197.
38 W. A. van der Donk and H. Zhao, *Curr. Opin. Biotechnol.*, 2003, **14**, 421–426.
39 H. Zhao and W. A. van der Donk, *Curr. Opin. Biotechnol.*, 2003, **14**, 583–589.
40 T. W. Johannes, R. D. Woodyer and H. Zhao, *Biotechnol. Bioeng.*, 2007, **96**, 18–26.
41 R. Woodyer, W. A. van der Donk and H. Zhao, *Comb. Chem. High Throughput Screening*, 2006, **9**, 237–245.
42 J. S. Griffith and L. E. Orgel, *Q. Rev., Chem. Soc.*, 1957, **11**, 381–393.
43 T. Lu and F. Chen, *J. Comput. Chem.*, 2012, **33**, 580–592.
44 J. Yu, Y. Zhou, I. Tanaka and M. Yao, *Bioinformatics*, 2010, **26**, 46–52.